Journal of Nuclear Medicine, published on January 11, 2018 as doi:10.2967/jnumed.117.199075

ImmunoPET in inflammatory bowel disease: Imaging CD4+ T cells in a murine model of colitis

Amanda C Freise[1,2], Kirstin A Zettlitz[1], Felix B Salazar[1], Richard Tavaré[1,3], Wen-Ting K Tsai[1], Arion F Chatziioannou[1], Nora Rozengurt[4], Jonathan Braun[1,4], Anna M Wu[1]

[1]Crump Institute for Molecular Imaging, Department of Molecular and Medical Pharmacology, David Geffen School of Medicine at UCLA
[2]Current affiliation: Department of Microbiology, Immunology, and Molecular Genetics, UCLA
[3]Current affiliation: Regeneron Pharmaceuticals, Inc., Tarrytown, New York
[4]Department of Pathology and Laboratory Medicine, David Geffen School of Medicine at UCLA

Corresponding author:

Anna M. Wu
Crump Institute for Molecular Imaging
University of California, Los Angeles
570 Westwood Plaza, CNSI 4335
PO Box 951770
Los Angeles, CA 90095-1770
USA

Tel: 1 (310) 794-5088
Fax: 1 (310) 206-8975
email: awu@mednet.ucla.edu

First author:

Amanda C. Freise
Department of Microbiology, Immunology, and Molecular Genetics
University of California, Los Angeles
609 Charles E. Young Drive East
3801A Molecular Science Building
Los Angeles, CA 90095-1489
USA

Tel: 1 (310) 206-5062

Email: afreise@ucla.edu

Word count: 5000

Running Title: Anti-CD4 immunoPET in colitic mice

Financial Support

This work was supported by NIH grants P30DK41301, P30CA016042, 5P30AI028697, P30CA016042, R21AI114255, and R25T098010.

ABSTRACT

Inflammatory bowel diseases (IBD) in humans are characterized in part by aberrant CD4+ T cell responses. Currently, identification of foci of inflammation within the gut requires invasive procedures such as colonoscopy and biopsy. Molecular imaging with antibody fragment probes could be used to noninvasively monitor cell subsets causing intestinal inflammation. Here, GK1.5 cys-diabody (cDb), an anti-mouse CD4 antibody fragment derived from the GK1.5 hybridoma, was used as a positron emission tomography (PET) probe for CD4+ T cells in the dextran sulfate sodium (DSS) mouse model of IBD.

METHODS: The DSS mouse model of IBD was validated by assessing changes in CD4+ T cells in the spleen and mesenteric lymph nodes (MLN) using flow cytometry. Furthermore, CD4+ T cell infiltration in the colons of colitic mice was evaluated using immunohistochemistry. ^{89}Zr-labelled GK1.5 cDb was used to image distribution of CD4+ T cells in the abdominal region and lymphoid organs of mice with DSS-induced colitis. Region of interest (ROI) analysis was performed on specific regions of the gut to quantify probe uptake. Colons, ceca, and MLN were removed and imaged *ex vivo* by PET. Imaging results were confirmed by *ex vivo* biodistribution analysis.

RESULTS: Increased number of CD4+ T cells in colons of colitic mice was confirmed by anti-CD4 immunohistochemistry. Increased uptake of ^{89}Zr-malDFO-GK1.5 cDb in the distal colon of colitic mice was visible *in vivo* in PET scans, and ROI analysis of the distal colon confirmed increased activity in DSS mice. MLN from colitic mice were enlarged and visible in PET images. *Ex vivo* scans and biodistribution confirmed higher uptake in DSS-treated colons (DSS: 1.8±0.40, control: 0.45±0.12 % injected dose (ID)/organ respectively), ceca (DSS: 1.1±0.38, control: 0.35±0.09 % ID/organ), and MLN (DSS: 1.1±0.58, control: 0.37±0.25 % ID/organ).

CONCLUSION: ^{89}Zr-malDFO-GK1.5 cDb detected CD4+ T cells in the colons, ceca, and MLN of colitic mice, and could prove useful for further investigations of CD4+ T cells in preclinical models of IBD, with potential to guide development of antibody-based imaging in human IBD.

Key words:

immunoPET; CD4; inflammatory bowel disease, zirconium-89; diabody

INTRODUCTION

The gut is a crucial compartment of the immune system. Lymphocytes reside in multiple locations throughout the gut including the intestine, gut-associated lymphoid tissue such as Peyer's patches and lymphoid follicles, and MLN (*1*). The immune system must balance the maintenance of tolerance to the many food- and microbiome-derived antigens sampled from the gut and mounting an immune response to pathogens. Dysregulation of this delicate balance can lead to IBD, a family of disorders characterized in part by abnormal and excessive T cell responses (*2*).

CD4+ T cells are known mediators of inflammation in IBD. Crohn's disease and ulcerative colitis each involve different subsets of CD4+ T cells, including Th1, Th2, and Th17 (*2*). Mouse models of IBD have helped advance understanding of how certain immune cell subsets, including CD4+ T cells, contribute to gut inflammation. Several models, such as the CD4+CD45RB^{hi} T cell transfer model and the 2,4,6-Trinitrobenzenesulfonic acid/oxalozone model, are CD4+ T cell-dependent and are used to study contributions of the adaptive immune system to IBD (*3*). The DSS model of colitis is often used to investigate innate immune cell contributions, as it is characterized by an initial influx of neutrophils, followed by infiltration of T cells. While CD4+ T cells are not required for the induction of DSS colitis (*4*,*5*), they do increase in number in the colon as the disease progresses (*6*). Hall et al. found that the peak number of

CD4+ T cells occurred on day 12 after initiation of DSS administration. In addition, changes in the percent of T cells in spleen and MLN can occur as early as day 1 (*6*), indicating that during acute colitis the adaptive immune system is already changing, even though T cells are not required for induction. Given these findings, continued investigation into the role of CD4+ T cells in the DSS colitis model is warranted.

Molecular imaging has been used to assess inflammation in murine models of colitis. ^{18}F-fluoro-deoxyglucose (FDG) and PET imaging were used in the DSS model to detect inflammation at several time points during progression of acute disease (*7*), and to correlate uptake in the colon with histologic damage and expression of perforin (*8*). FDG-PET was utilized to identify inflammation in models with mild or severe chronic colitis, including the $CD4^{+}CD45RB^{high}$ and $G\alpha i2^{-/-}CD3^{+}$ T cell transfer models (*9*). In humans with IBD, FDG-PET can identify inflammation with estimated sensitivity of 85% and specificity of 87% (*10*) and provide information complementary to standard methods such as colonoscopy and clinical symptom tracking (*11*); one caveat is that physiological uptake of FDG-PET in the gut is highly variable which may reduce its utility as a screening tool (*12*).

Investigating specific cell subsets involved in IBD requires more specific probes. Molecular imaging with antibodies enables imaging of cell-surface biomarkers (*13*), and antibodies have been used to image immune cells in models

of colitis. Kanwar et al. used a non-depleting intact anti-CD4 antibody for single-photon emission computed tomography imaging of CD4+ T cells in DSS colitis, and showed that uptake in the lower abdomen correlated with disease severity and the number of CD4+ T cells present (*14*). The integrin β_7 subunit, expressed on lymphocytes activated in Peyer's patches and MLN, was recently used as a target for single-photon emission computed tomography imaging in DSS-treated colitic mice (*15*). Dearling et al. developed fragments of the anti-integrin β_7 antibody probe and used them to image lymphocytes in the intestines of colitic mice (16).

We previously described GK1.5 cDb, an anti-mouse CD4 antibody fragment, and demonstrated its use in tracking immune system reconstitution post-hematopoietic stem cell transplant (*17*). Subsequent studies investigated the effect of protein dose on image contrast and biological effect on CD4+ T cells, and showed that low-dose GK1.5 cDb produces high-contrast images of lymphoid organs with minimal effects on CD4+ T cell function *in vivo* (*18*). Here, the utility of anti-CD4 GK1.5 cDb as an immunoPET probe for regions of CD4+ T cell infiltration in the murine DSS model of IBD has been evaluated, and correlated with *ex vivo* biodistribution analysis, flow cytometry, and immunohistochemistry of CD4+ T cells in the intestines and lymphoid organs.

MATERIALS AND METHODS

Animals

Female C57BL/6 mice 6-12 weeks of age were obtained from Jackson Laboratories and housed by the Department of Laboratory Animal Medicine at the University of California, Los Angeles under specific pathogen-free conditions. Animal studies were conducted under protocols approved by the institutional Chancellor's Animal Research Committee.

Induction and Assessment of Colitis

DSS (40,000 kDa, Sigma) was dissolved in autoclaved tap water, sterile filtered, and provided *ad libitum*. Based on published literature (*6*) and dose-finding pilot studies (data not shown), we determined that 4% DSS administered for five days induced infiltration of mononuclear cells into the colon by day 12. Regular water was restored on day 6. Mice were weighed every day and examined for signs of colitis, evaluated by a disease activity index modified from Sha *et al.* (*19)*: Weight loss (0: none, 1: 1–4%, 2: 5–10%, 3: 11-20% 4: >20%), fecal blood (0: none, 2: blood present in stool, 4: gross bleeding from anus), and stool consistency (0: normal, 2: loose stools, 4: diarrhea). On day 12, mice were euthanized and the colon, cecum, and MLN were removed. MLN were pooled per individual mouse, weighed, and divided by number of MLN collected to get the average weight of one MLN for each mouse.

GK1.5 cDb Administration and PET/CT Imaging

Anti-mouse CD4 GK1.5 cDb was produced, purified, and radiolabeled as described previously (*17*,*18*).

^{89}Zr-malDFO-GK1.5 cDb (2 μg; 0.38 MBq) was injected intravenously. One hour before imaging, 100 μl Gastrografin (diatrizoate meglumine and diatrizoate sodium solution; Bracco) was administered orally for CT contrast of the upper gastrointestinal tract. Immediately prior to imaging, mice were anesthetized with 2% isoflurane and 100 μl Gastrografin was administered intrarectally for large intestine contrast. PET and CT scans were acquired 20 h post-injection as previously described (*18*). CT scans were acquired on the CrumpCAT, a fast microCT prototype developed at our institution (*20*). *Ex vivo* PET/CT scans of harvested colons, ceca, and MLN were acquired using the same parameters as above. PET/CT images were viewed using AMIDE (http://amide.sourceforge.net). Biodistribution analysis was conducted as previously described (*18*). Additionally, colons and ceca were fixed and processed for histopathological and immunohistochemical analysis.

For quantitative analysis of intestinal uptake, first the skeleton was manually removed from the CT image using several regions of interest (ROI). A 3D isocontour ROI around the contrast-enhanced small and large intestines ("gut ROI") was created. After gut ROI quantification, a cylindrical ROI was drawn around a representative colon, from the anus to just below the kidneys, and used

on every mouse to reproducibly crop out the same amount of anatomy. A 3D isocontour ROI was then drawn on the remaining distal colon and quantified.

Flow Cytometry

Lymphocytes in MLN and spleens were analyzed by flow cytometry. Organ harvesting and preparation was performed as described previously (*18*).

Statistical Analysis

Prism software (GraphPad) was used to perform two-tailed Student's T tests. A p-value of less than 0.05 was considered to be statistically significant. For T tests on organs from the *ex vivo* biodistribution study, the Holm-Sidak correction for multiple comparisons was applied. Values are reported as mean ± standard deviation unless indicated otherwise.

RESULTS

DSS-Induced Colitis Results in Gross Anatomical Changes

Mice treated with 4% DSS for 5 days (Fig. 1A) showed weight loss beginning on day 6. On day 12, the weight of DSS-treated mice was significantly reduced to 87 ± 0.06 % of initial weight, whereas control mice did not display any weight loss ($p<0.0001$; $n=8$) (Fig. 1B). DSS-treated mice also had significantly

higher scores on the disease activity index compared to control mice as a result of increased weight loss, loose stool, and fecal bleeding (Supplemental Fig. 1A).

Colons from DSS-treated mice were significantly shorter ($p<0.05$) (Fig. 1C) and heavier (data not shown) than control colons. The colon weight:length ratio was significantly higher in colitic mice ($p<0.001$) (Fig. 1D). Individual MLN from DSS-treated mice weighed more on average (6.1 ± 3.0 mg; range: 1.4-11) compared to MLN from control mice (2.1 ± 1.1 mg; range: 0.4-4.4; $p<0.0001$; n=8 mice) (Fig. 1E); furthermore, average MLN cellularity was higher in DSS mice (n=4 mice; Supplemental Fig. 2).

Histopathological analysis showed that colons from DSS-treated mice had epithelial cell loss, crypt destruction, and infiltration of inflammatory cells into the mucosa (Supplemental Figs. 1B and 1C). These signs were severe but localized in most mice. DSS-treated mice also had significantly more lymphoid aggregates throughout the colon (Supplemental Fig. 1D).

Changes in CD4+ T Cells in DSS-Treated Mice

Anti-CD4 immunohistochemical staining showed increased infiltration of CD4+ T cells into the colons of DSS-treated mice (Fig. 2A). $CD4^+$ cells were on average 0.66 ± 0.46 % of the total cells in each section of colon in control mice, whereas DSS-treated mice had an average of 1.9 ± 1.5 % $CD4^+$ cells ($p<0.05$; control n=12, DSS n=13) (Fig. 2B). Ceca from colitic mice did not show a

significant increase in the percent of CD4+ T cells (Supplemental Fig. 3A). Changes in CD4+ T cells in spleen and MLN were evaluated by flow cytometry. The percent of CD45+CD4+ cells in the spleen increased slightly in DSS mice, though not significantly (control: 20.6±4.4 %; DSS: 23.7±4.1 %; n=11 mice) (Supplemental Fig. 3B). The percent of CD45+CD4+ cells in MLN of DSS mice decreased significantly (control: 33.0±9.4 %; DSS: 24.6±6.1 %; $p<0.05$; control: n=9 mice, DSS: n=10 mice) (Fig. 2C).

ImmunoPET Imaging of CD4 in Colitic Mice

GK1.5 cDb was site-specifically conjugated to malDFO and radiolabeled with ^{89}Zr. Radiolabeling efficiency was >99% (n=3). Specific activity was 0.19±0.023 MBq/μg ($9.9x10^5$±$1.2x10^5$ MBq/mmol), and radiochemical purity was >99% (n=3). ^{89}Zr-malDFO-GK1.5 cDb (2 μg; 0.38 MBq) was injected into groups of mice (two experiments of n=4 mice/group). PET imaging showed tracer uptake in spleens and lymph nodes, consistent with previous results of studies of untreated mice (*18*) (Fig. 3A). PET scans of colitic mice demonstrated increased signal from MLN. The colons of colitic mice also showed uptake of ^{89}Zr-malDFO-GK1.5 cDb, whereas the control mice show little to no uptake in the colon (Fig. 3A). Oral and intrarectal instillation of CT contrast agent delineated the intestine clearly on the CT scan (Supplemental Figs. 4A and 4B) and enabled 3D isocontour ROIs of the complete small and large intestines (gut ROI) and of

the distal colon only (colon ROI) to be created based on intensity of CT signal after manual removal of the skeleton (Supplemental Fig. 4C; Fig. 3B). DSS mice had significantly increased uptake in the colon ROI ($p<0.005$) but not the gut ROI compared to control mice ($p=0.548$) (Fig. 3C); spillover signal from the kidneys into the ROI may have masked actual differences.

Ex vivo scans confirmed the results of in the *in vivo* scans, showing visibly increased uptake in colons, ceca, and MLN from DSS mice (Fig. 4). Biodistribution studies showed that total activity was higher in DSS-treated colons, ceca, and MLN (3.1-fold, 3.9-fold, and 3.0 fold, respectively) (Fig. 5A; Table 1). Comparing concentration of activity (%ID/g) in organs known to be affected by DSS-induced colitis (colon, cecum, and MLN) did not result in significant changes in uptake (Fig. 5B; Supplemental Table 1).

DISCUSSION

Aberrant activation and infiltration of CD4+ T cells is a hallmark of IBD in humans, and in numerous mouse models of IBD. The contribution of CD4+ T cells to DSS colitis is still controversial. Although the DSS model does not require T cells for induction of colitis (*4,5*), they still infiltrate into the colon (*6*), and CD4+ T cells appear to play a role in the chronic stage of colitis (*21, 22*). Adoptive transfer of DSS-primed CD4+ T cells into recipient mice treated with DSS resulted in exaggerated colitis (*23*). Conversely, athymic CD-1 nu/nu mice

treated with DSS developed more severe clinical signs of colitis than normal mice, suggesting that T cells may be protective in DSS colitis (*5*). Molecular imaging could be of use to further investigate how CD4+ T cells affect the induction and progression of DSS colitis.

The DSS model and resulting changes in CD4+ T cells were validated using quantitative immunohistochemistry and flow cytometry. Radiolabeled anti-CD4 GK1.5 cDb was used to see if the presence of increased CD4+ T cells could be visualized and quantified with immunoPET. ^{89}Zr-malDFO-GK1.5 cDb successfully detected CD4+ T cells in the colons and MLN of colitic mice, and quantification of the distal colon region with ROI analysis showed that uptake significantly increased in colitic mice. This result is consistent with other studies which report that the most severe damage in the DSS model occurs in that region (*4,24*). Quantifying uptake in the gut ROI, which included both the small and large intestines, was challenging because the probe cleared through the kidneys, resulting in signal spillover into the anterior region of the ROI; differences in the gut ROI values were not significant between control and DSS-treated mice.

Significantly increased uptake of ^{89}Zr-malDFO-GK1.5 cDb in the distal colon ROI, as well as in MLN, was supported by the *ex vivo* organ scans. Interestingly, uptake was also increased in the ceca of colitic mice, although we did not observe increased CD4+ T cells by immunohistochemistry in colitic ceca; this may be due at least in part to enhanced permeability of the cecum due to

DSS-induced inflammation. Quantification of uptake via *ex vivo* biodistribution analysis confirmed a significant increase in % ID/organ for colons, MLN, and ceca of DSS-treated mice; however, the concentration of activity in these organs (presented as % ID/g) was not significantly higher in DSS mice. In colons of DSS mice, this may be explained by the finding that they were heavier than control colons. In DSS-treated MLN, although the percent of CD4+ T cells decreased, MLN were significantly enlarged which suggests that both CD4+ T cells *and* other types of immune cells were present in higher total numbers, resulting in increased size but not increased concentration.

In *in situ* and *ex vivo* immunoPET images, colitic MLN appear to have higher % ID/g than control MLN, but *ex vivo* biodistribution analysis indicates that they have the same % ID/g. This finding is explained by the partial volume effect, in which the concentration of activity in organs near the resolution of the PET scanner is underestimated (*17*). Colitic MLN were dramatically enlarged and more easily detected by immunoPET compared to the tiny control MLN. The partial volume effect, especially in the context of murine lymph nodes, has been observed and discussed in previous work from our laboratory (*17*). The observation of signal from enlarged MLN in colitic mice demonstrates the importance of MLN and associated lymphatics in the development of DSS colitis and raises the possibility of the prognostic value of inflammatory staging sites

such as MLN, though more work is needed to fully understand the timing and cellular dynamics of MLN enlargement.

These results confirm and expand on the work of Kanwar *et al*., who employed indium-111-labeled intact anti-CD4 antibody for single-photon emission computed tomography imaging of CD4+ T cells in DSS mice; in that work, a protein dose of 350 μg was used (*14*). We previously explored protein doses and found that amounts as low as 2 μg GK1.5 cDb enabled imaging CD4+ T cells in the lymph nodes and spleen with minimal biological effects (*18*). Here, 2 μg GK1.5 cDb was sufficient to image CD4+ T cells in the DSS model. Furthermore, Kanwar *et al*. drew an ROI that encompassed the entire lower abdomen and referred to this as "colon uptake" but did not discuss signal from CD4+ T cells in the MLN (*14*), which were likely included in the ROI. Therefore, while whole-abdomen ROIs may have prognostic value in IBD, they must be interpreted with consideration of the presence of MLN and associated lymphatic tissue.

While GK1.5 cDb enables visualization of total CD4+ cells in the gut, it does not provide information about CD4+ T cell subsets such as Th1, Th2, Th17, or Tregs, which is disadvantageous given the different pro- and anti-inflammatory roles of each of these subsets. However, GK1.5 cDb can be used to identify sites of CD4+ T cell accumulation, followed by detailed analysis with traditional methods such as biopsy to determine the subsets present as needed. Further

studies using GK1.5 cDb in mouse models of IBD could include imaging CD4 in a T-cell dependent model or imaging at several time points during the development of colitis to investigate the course of T cell infiltration into the intestines and MLN.

CD4+ T cells play a key role in human IBD, and identifying them throughout the bowel could be useful to monitor disease severity and predict treatment success. Imaging is less intrusive than colonoscopies, which are uncomfortable for patients and carry a risk of bowel perforation; furthermore, inflammation can vary depending on the position within the bowel. Anti-CD4 immunoPET could provide an overview of inflammatory sites throughout the intestines. Other immune targets, including granulocytes (*24*), E-selectin (*25*), and CXCL8 (*12*), have been imaged in IBD patients. Aarntzen et al. suggest that anti-CXCL8 imaging could be a tool for making decisions about immune-modulating treatment (*12*); a similar application could apply for anti-CD4 imaging.

CONCLUSION

Anti-CD4 immunoPET with GK1.5 cDb enabled detection of CD4+ T cells in inflamed mouse colons and in enlarged MLN, and should provide a useful tool for investigating CD4+ T cells in murine models of IBD and other diseases with a CD4 inflammatory component.

Financial Disclosure

A. M. W. is a stockholder in and consultant to ImaginAb, Inc.

ACKNOWLEDGMENTS

We thank Kha Huynh, Alec Estrada, Waldemar Ladno, Theresa Falls, Jason Lee, Richard Taschereau, and Clara Magyar for technical assistance. Histological analysis was provided by the UCLA Imaging and Stem Cell Core at the CURE Digestive Diseases Research Center (NIH P30DK41301). Flow cytometry was performed in the UCLA Jonsson Comprehensive Cancer Center (JCCC) and Center for AIDS Research Flow Cytometry Core Facility (NIH P30CA016042 and 5P30AI028697). MicroPET scans were performed in the Preclinical Imaging Technology Core at the Crump Institute for Molecular Imaging at UCLA, which is funded by the UCLA JCCC and National Institutes of Health (NIH P30CA016042). A. C. F. was supported by the Dissertation Year Fellowship from UCLA. R. T. was funded by NIH award R21AI114255 and the UCLA Scholars in Oncologic Molecular Imaging training program (NIH R25T098010). A. M. W. is a member of the JCCC.

REFERENCES

1. Brandtzaeg P, Kiyono H, Pabst R, Russell MW. Terminology: nomenclature of mucosa-associated lymphoid tissue. *Mucosal Immunol*. 2008;1:31-37.
2. Geremia A, Biancheri P, Allan P, Corazza GR, Di Sabatino A. Innate and adaptive immunity in inflammatory bowel disease. *Autoimmun Rev*. 2014;13:3-10.
3. Wirtz S, Neurath MF. Mouse models of inflammatory bowel disease. *Adv Drug Deliv Rev*. 2007;59:1073-1083.
4. Dieleman LA, Ridwan BU, Tennyson GS, Beagley KW, Bucy RP, Elson CO. Dextran sulfate sodium-induced colitis occurs in severe combined immunodeficient mice. *Gastroenterology*. 1994;107:1643-1652.
5. Axelsson LG, Landström E, Goldschmidt TJ, Grönberg A, Bylund-Fellenius AC. Dextran sulfate sodium (DSS) induced experimental colitis in immunodeficient mice: effects in CD4+ -cell depleted, athymic and NK-cell depleted SCID mice. *Inflamm Res*. 1996;45:181-191.
6. Hall LJ, Faivre E, Quinlan A, Shanahan F, Nally K, Melgar S. Induction and activation of adaptive immune populations during acute and chronic phases of a murine model of experimental colitis. *Dig Dis Sci*. 2011;56:79-89.
7. Hindryckx P, Staelens S, Devisscher L, et al. Longitudinal quantification of

inflammation in the murine dextran sodium sulfate-induced colitis model using microPET/CT. *Inflamm Bowel Dis*. 2011;17:2058-2064.

8. Bettenworth D, Reuter S, Hermann S, et al. Translational ^{18}F-FDG PET/CT imaging to monitor lesion activity in intestinal inflammation. *J Nucl Med*. 2013;54:748-755.

9. Brewer S, McPherson M, Fujiwara D, et al. Molecular imaging of murine intestinal inflammation with 2-deoxy-2-[^{18}F]fluoro-D-glucose and positron emission tomography. *Gastroenterology*. 2008;135:744-755.

10. Treglia G, Quartuccio N, Sadeghi R, et al. Diagnostic performance of fluorine-18-fluorodeoxyglucose positron emission tomography in patients with chronic inflammatory bowel disease: a systematic review and a meta-analysis. *J Crohn's Colitis*. 2013;7:345-354.

11. Glaudemans AWJM, de Vries EFJ, Galli F, Dierckx RAJO, Slart RHJA, Signore A. The use of ^{18}F-FDG-PET/CT for diagnosis and treatment monitoring of inflammatory and infectious diseases. *Clin Dev Immunol*. 2013;2013:1-14.

12. Aarntzen EHJG, Hermsen R, Drenth JPH, Boerman OC, Oyen WJG. ^{99m}Tc-CXCL8 SPECT to monitor disease activity in inflammatory bowel disease. *J Nucl Med*. 2016;57:398-403.

13. Freise AC, Wu AM. In vivo imaging with antibodies and engineered fragments. *Mol Immunol*. 2015;67:142-152.

14. Kanwar B, Gao DW, Hwang AB, et al. In vivo imaging of mucosal CD4+ T cells using single photon emission computed tomography in a murine model of colitis. *J Immunol Methods*. 2008;329:21-30.

15. Dearling JLJ, Park EJ, Dunning P, et al. Detection of intestinal inflammation by microPET imaging using a ^{64}Cu-labeled anti-beta7 integrin antibody. *Inflamm Bowel Dis*. 2010;16:1458-1466.

16. Dearling JLJ, Daka A, Veiga N, Peer D, Packard AB. Colitis immunoPET: defining target cell populations and optimizing pharmacokinetics. *Inflamm Bowel Dis*. 2016;22:529-538.

17. Tavaré R, McCracken MN, Zettlitz KA, Salazar FB, Witte ON, Wu AM. ImmunoPET of murine T cell reconstitution post-adoptive stem cell transplant using anti-CD4 and anti-CD8 cys-diabodies. *J Nucl Med*. 2015;56:1258-1264.

18. Freise AC, Zettlitz KA, Salazar FB, Lu X, Tavaré R, Wu AM. ImmunoPET Imaging of murine CD4+ T cells using anti-CD4 cys-diabody: effects of protein dose on T cell function and imaging. *Mol Imaging Biol*. 2017;19:599-609.

19. Sha T, Igaki K, Yamasaki M, Watanabe T, Tsuchimori N. Establishment and validation of a new semi-chronic dextran sulfate sodium-induced model of colitis in mice. *Int Immunopharmacol*. 2013;15:23-29.

20. Taschereau R, Vu NT, Chatziioannou AF (2014) Calibration and data standardization of a prototype bench-top preclinical CT. Presented at: IEEE Nuclear Science Symposium and Medical Imaging Conference, November 8-15, 2014, Seattle, WA, USA. Abstract 15853923.

21. Dieleman LA, Palmen MJ, Akol H, et al. Chronic experimental colitis induced by dextran sulphate sodium (DSS) is characterized by Th1 and Th2 cytokines. *Clin Exp Immunol*. 1998;114:385-391.

22. Melgar S, Karlsson A, Michaëlsson E. Acute colitis induced by dextran sulfate sodium progresses to chronicity in C57BL/6 but not in BALB/c mice: correlation between symptoms and inflammation. *Am J Physiol Gastrointest Liver Physiol*. 2005;288:G1328-G1338.

23. Shintani N, Nakajima T, Okamoto T, Kondo T, Nakamura N, Mayumi T. Involvement of CD4+ T cells in the development of dextran sulfate sodium-induced experimental colitis and suppressive effect of IgG on their action. *Gen Pharmacol*. 1998;31:477-481.

24. Kitajima S, Takuma S, Morimoto M. Tissue distribution of dextran sulfate sodium (DSS) in the acute phase of murine DSS-induced colitis. *J Vet Med Sci*. 1999;61:67-70.

25. Bruno I, Martelossi S, Geatti O, et al. Antigranulocyte monoclonal antibody immunoscintigraphy in inflammatory bowel disease in children and young adolescents. *Acta Paediatr*. 2002;91:1050-1055.

26. Bhatti M, Chapman P, Peters M, Haskard D, Hodgson HJF. Visualising E-selectin in the detection and evaluation of inflammatory bowel disease. *Gut*. 1998;43:40-47.

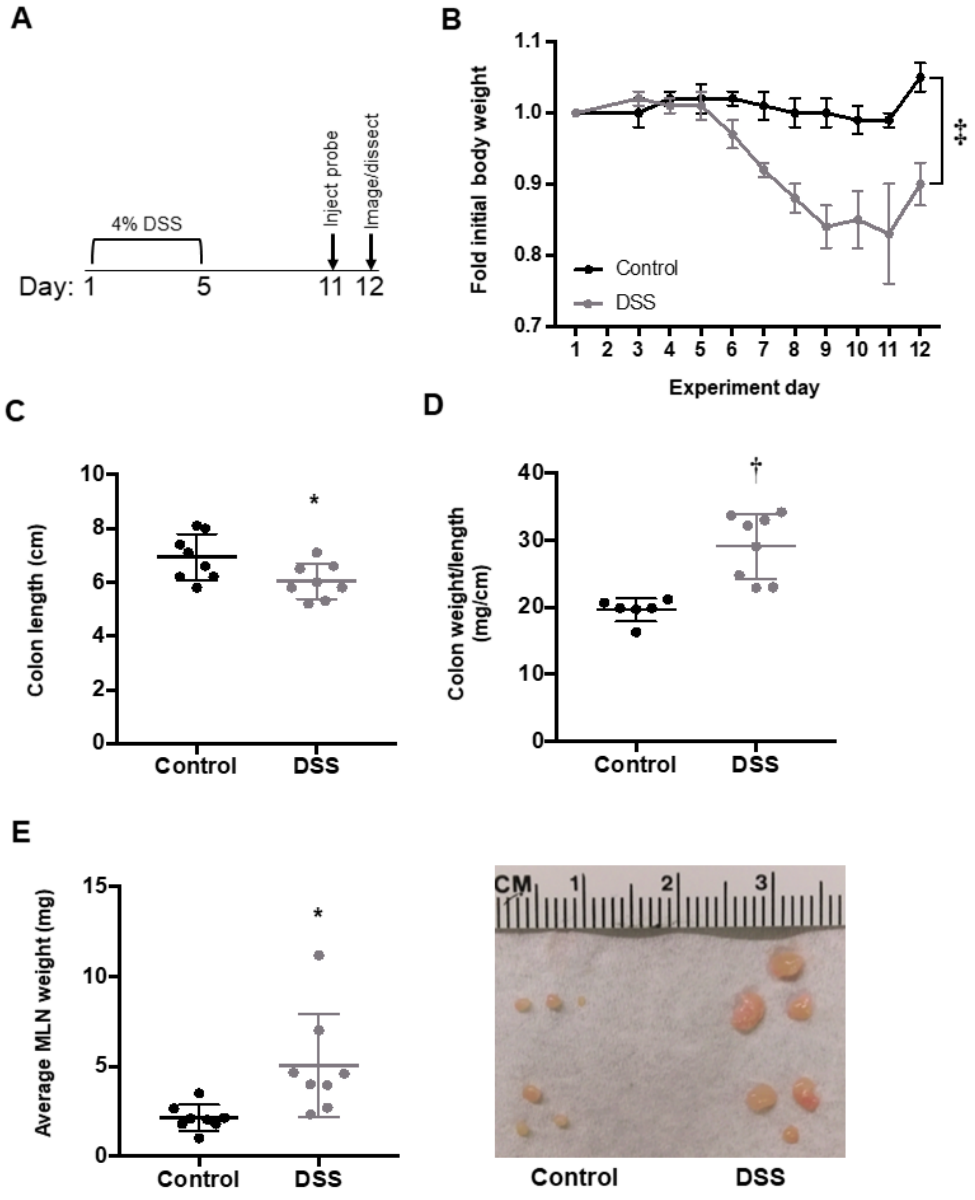

FIGURE 1 Characterization of DSS-induced anatomical changes in colitic mice

(A) Schematic showing days of DSS treatment, injection of ^{89}Zr-malDFO-GK1.5 cDb, and PET imaging. (B) Change in body weight during and after DSS

treatment (n=8). (C) Colons were cut just below the cecum, laid flat, and measured (n=8). (D) Ratio of colon weight (after removing stool) to length (n=8). (E) MLN were removed, counted, pooled per mouse, and weighed. Each dot represents the average weight of one MLN from an individual mouse (n=8 mice). Image shows three representative MLN from two control mice (left) and two DSS-treated mice (right). * $p<0.05$, † $p<0.0005$, ‡ $p<0.0001$.

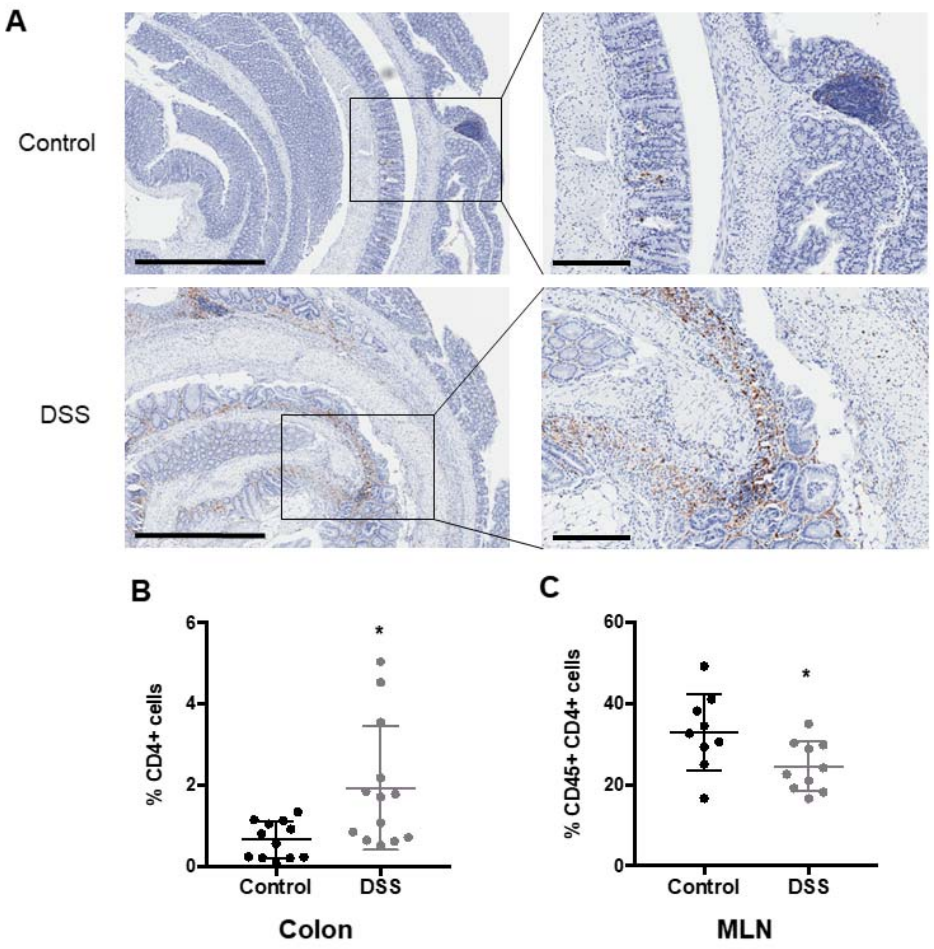

FIGURE 2 Characterization of CD4 cells in colons and MLN of DSS-treated mice

(A) Representative images of anti-mouse CD4 immunohistochemical staining in colons from control (top) and DSS-treated (bottom) mice. Left panels: 4X magnification; scale bar: 500 μm. Right panels: 10X magnification; scale bar: 200 μm. (B) The number of cells staining positive for CD4 from an entire colon section was divided by the total number of cells. Two sections of colon, 100 μm

apart, were analyzed per mouse; each point represents the average percent of CD4+ T cells in the colon from one mouse (control: n=12 mice, DSS: n=13). (C) Flow cytometric analysis of CD45+CD4+ cells from MLN (control: n=9; DSS: n=10) of control and DSS-treated mice. * $p<0.05$.

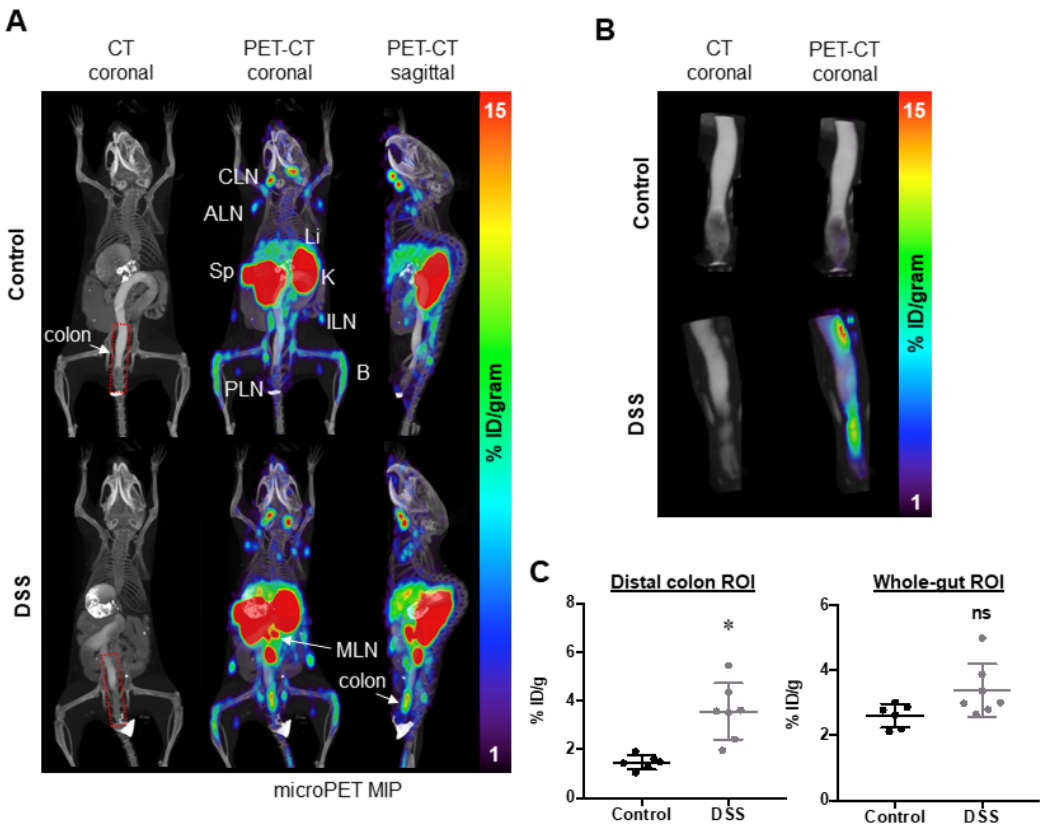

FIGURE 3 Anti-CD4 immunoPET of control and DSS-treated mice

(A) Representative CT (coronal view) and PET-CT (coronal and sagittal) images of control (top) and DSS-treated (bottom) mice imaged with 2 µg (0.34 MBq) ^{89}Zr-malDFO-GK1.5 cDb (n=8). Images were acquired 20 h post-injection of probe and are displayed as 25 mm maximum-intensity projections. Organs of interest are labeled: axillary LN (ALN), bone (B), cervical LN (CLN), inguinal LN (ILN), kidney (K), liver (Li), popliteal LN (PLN), mesenteric LN (MLN), spleen (Sp). The distal colon ROI is indicated by the red dotted line. (B) Representative CT and PET-CT images of the ROI drawn around the distal colon

from control (top) and DSS-treated (bottom) mice. (C) Quantitative analysis of ROIs drawn around the distal colon or the small and large intestines, using the 3D isocontour ROI function of AMIDE (control: n=6, DSS: n=7). * $p<0.005$.

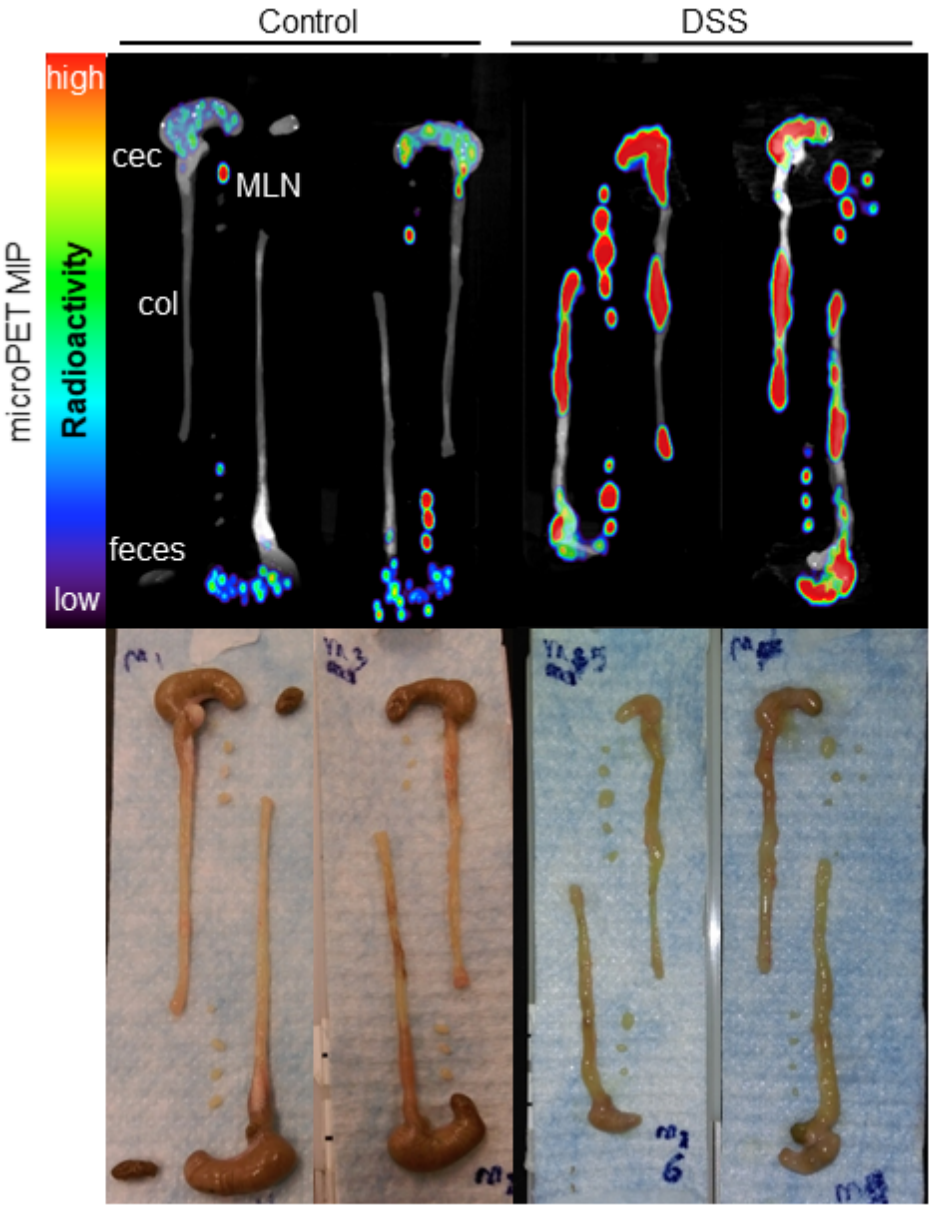

FIGURE 4 *Ex vivo* immunoPET images of colons, ceca, and mesenteric lymph nodes

After the *in vivo* PET/CT scan mice were euthanized, colons, ceca, and MLN were dissected and laid out for the *ex vivo* PET/CT scan (n=8 mice/group). Representative images are shown, displayed as 12 mm maximum-intensity projections.

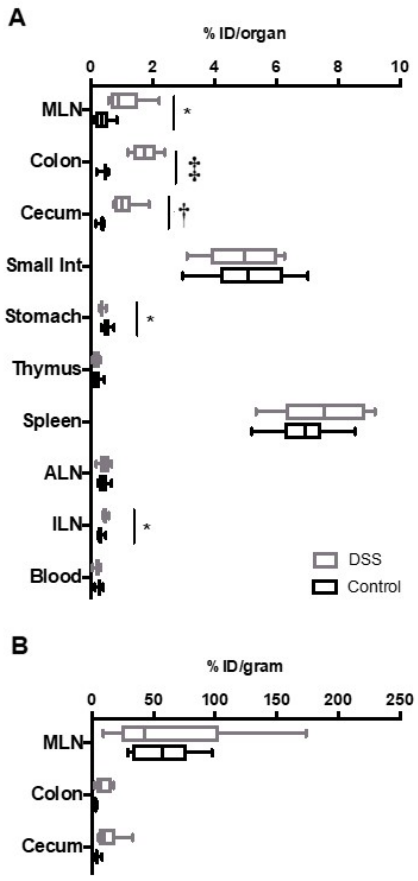

FIGURE 5 *Ex vivo* biodistribution of organs from control and DSS-treated mice

After the PET scan, mice were euthanized, and blood and organs were removed, weighed, and counted. Decay-corrected values for uptake are displayed. (A) %ID/organ for lymphoid and gastrointestinal organs. * $p<0.05$, †# $p<0.005$, ‡ $p<0.0001$. (B) %ID/gram for organs of interest: colon, cecum, and MLN (n=8). Box shows 25% quartile, median, and 75% quartiles. Whiskers indicate minimum and maximum values.

TABLE 1: *Ex vivo* biodistribution, % injected dose/organ

	Percent injected dose per organ (%ID/organ)					
	Control			DSS		
	Mean	SD	n	Mean	SD	n
MLN	0.37	0.25	8	1.09 *	0.58	8
Colon	0.45	0.12	8	1.75 ‡	0.40	8
Cecum	0.35	0.09	8	1.09 †	0.38	8
Small Int	5.12	1.33	8	4.87	1.13	8
Stomach	0.53	0.13	8	0.37 *	0.07	8
Thymus	0.17	0.14	8	0.16	0.11	8
Spleen	6.89	0.98	8	7.56	1.38	8
ALN	0.41	0.14	8	0.45	0.17	8
ILN	0.31	0.09	8	0.46 *	0.07	8
Blood	0.28	0.08	8	0.22	0.08	8
Liver	9.84	2.64	8	13.37	1.01	8
Kidney	23.84	6.26	8	27.30	3.68	8
Heart	0.15	0.04	8	0.21	0.07	8
Lung	0.38	0.26	8	0.36	0.03	8
Muscle	0.04	0.01	8	0.05	0.01	8
Femur	0.69	0.17	8	0.49	0.10	8
Tail	4.19	3.63	8	3.25	0.72	8
Carcass	19.53	3.24	8	16.64	0.96	8

Total activity present in blood and organs from DSS-treated mice was compared to those from control mice 26 h post-injection of ^{89}Zr-malDFO-GK1.5 cDb. * $p<0.05$, † $p<0.005$, ‡ $p<0.0001$. Abbreviations: axillary LN (ALN), inguinal LN (ILN), mesenteric LN (MLN).

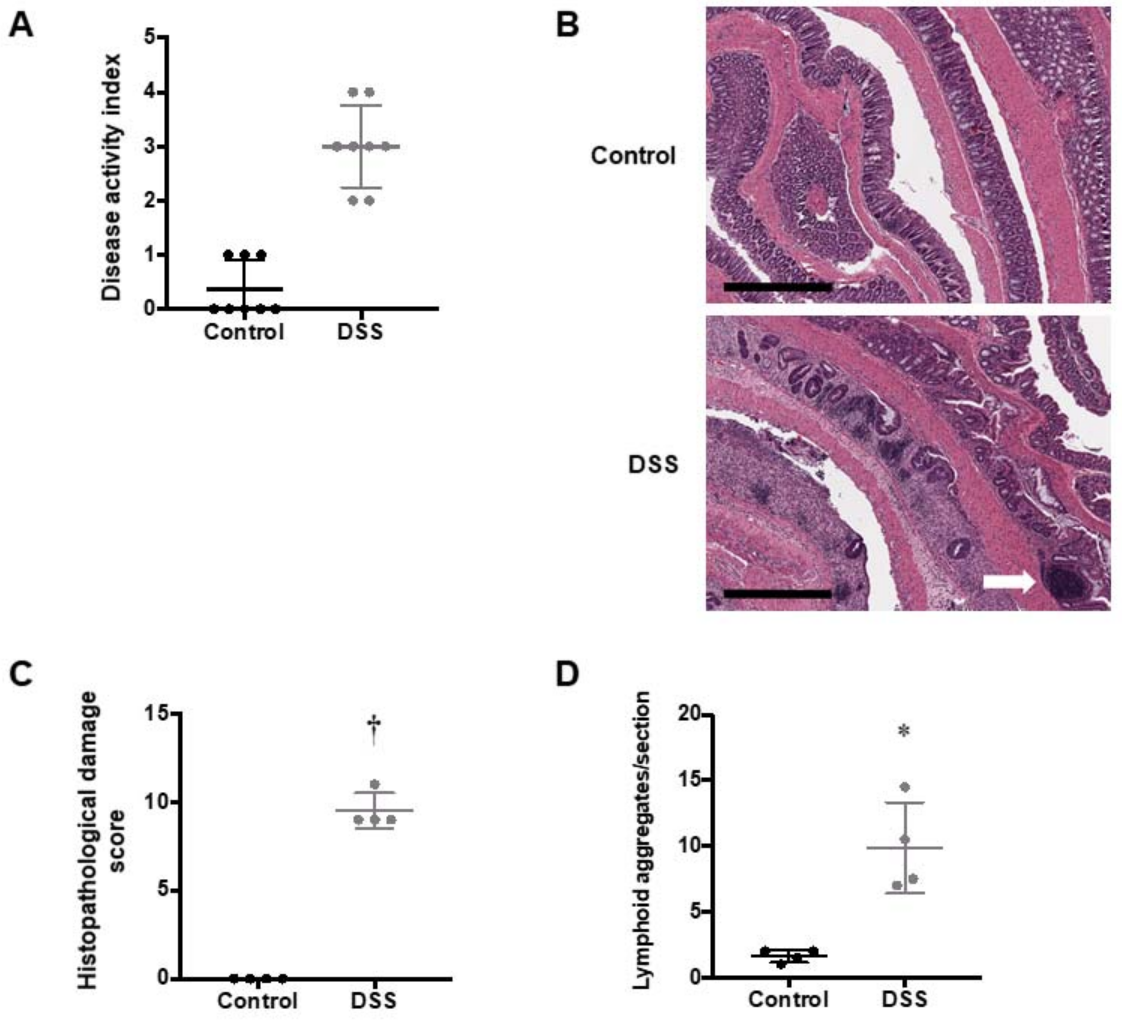

SUPPLEMENTAL FIGURE 1 Histopathological analysis of control and DSS-treated colons

(A) Clinical symptoms were quantified using the disease activity index, which scored symptoms including weight loss, stool consistency, and fecal bleeding, at the time of sacrifice (n=8). (B) Representative images of hematoxylin and eosin-stained 4 μm sections of colonic Swiss rolls from control (left) and DSS-treated (right) mice. A lymphoid aggregate is denoted with a white arrow. Magnified 4X; scale bar: 500 μm. (C) Histopathological damage as determined by severity of surface epithelial loss, crypt destruction, and inflammatory cell infiltration into

mucosa was quantified on 4 μm Swiss roll sections of colon tissue. Damage was quantified as follows: 0: normal, 1: localized and mild, 2: localized and moderate, 3: localized and severe, 4: extensive and moderate. (n=4). (D) Lymphoid aggregates (including normal gut-associated lymphoid tissues and tertiary lymphoid structures) in each section of colon were counted (n=4). * $p<0.005$, † $p<0.0001$.

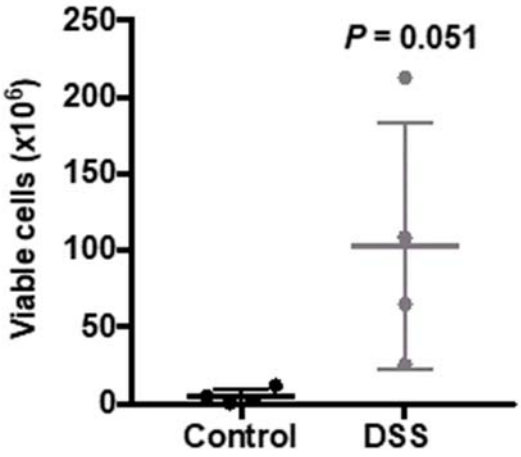

SUPPLEMENTAL FIGURE 2 MLN cellularity

To determine cellularity, two MLN were mashed gently through a 70 μm nylon filter, rinsed with 2.5ml PBS/2% FBS, and viable cells were enumerated using a Vi-Cell XR automatic cell counter (Beckman Coulter). Each point represents the average value of two MLN from a single control or DSS-treated mouse (n=4 mice).

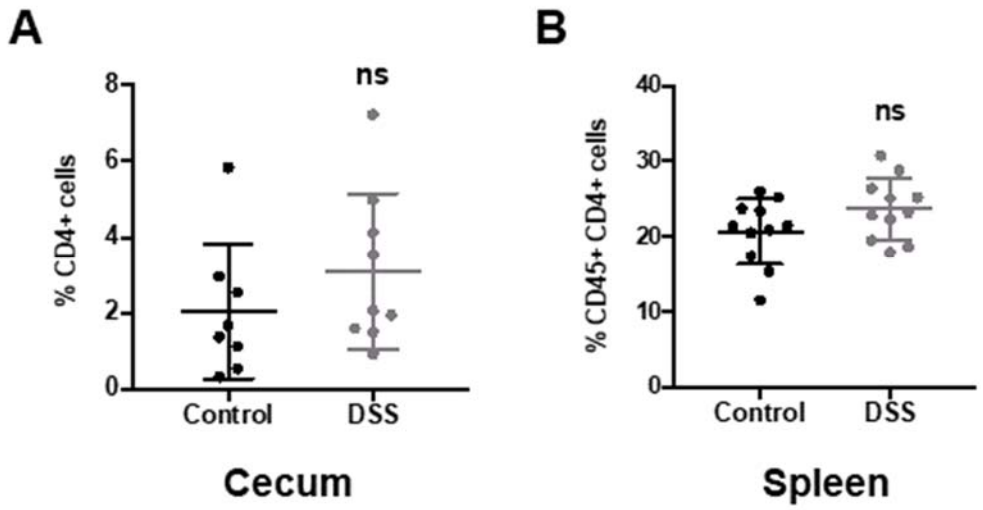

SUPPLEMENTAL FIGURE 3 Analysis of CD4-positive cells in cecum and spleen

(A) CD4 cells were visualized in the cecum with immunohistochemical staining. Slides were prepared by incubating sections with rabbit monoclonal anti-mouse CD4 antibody (Abcam), and CD4 was visualized with HRP-conjugated anti-rabbit antibody and 3,3'-diaminobenzidine. Slides were scanned on an Aperio ScanScope AT (Leica). Images were viewed using Aperio ImageScope software (Leica) and analyzed using Tissue Studio image analysis software (Definiens). The number of cells staining positive for CD4 from an entire 4 µm Swiss roll section of cecum was divided by the total number of cells. Two sections, separated by 100 µm, were cut and quantified per cecum; each point represents the average percent of CD4+ T cells in the colon from one mouse (n=8 mice). (B) Flow cytometric analysis of CD45+CD4+ cells from spleens of control and DSS-treated mice (n=11). ns: not significant.

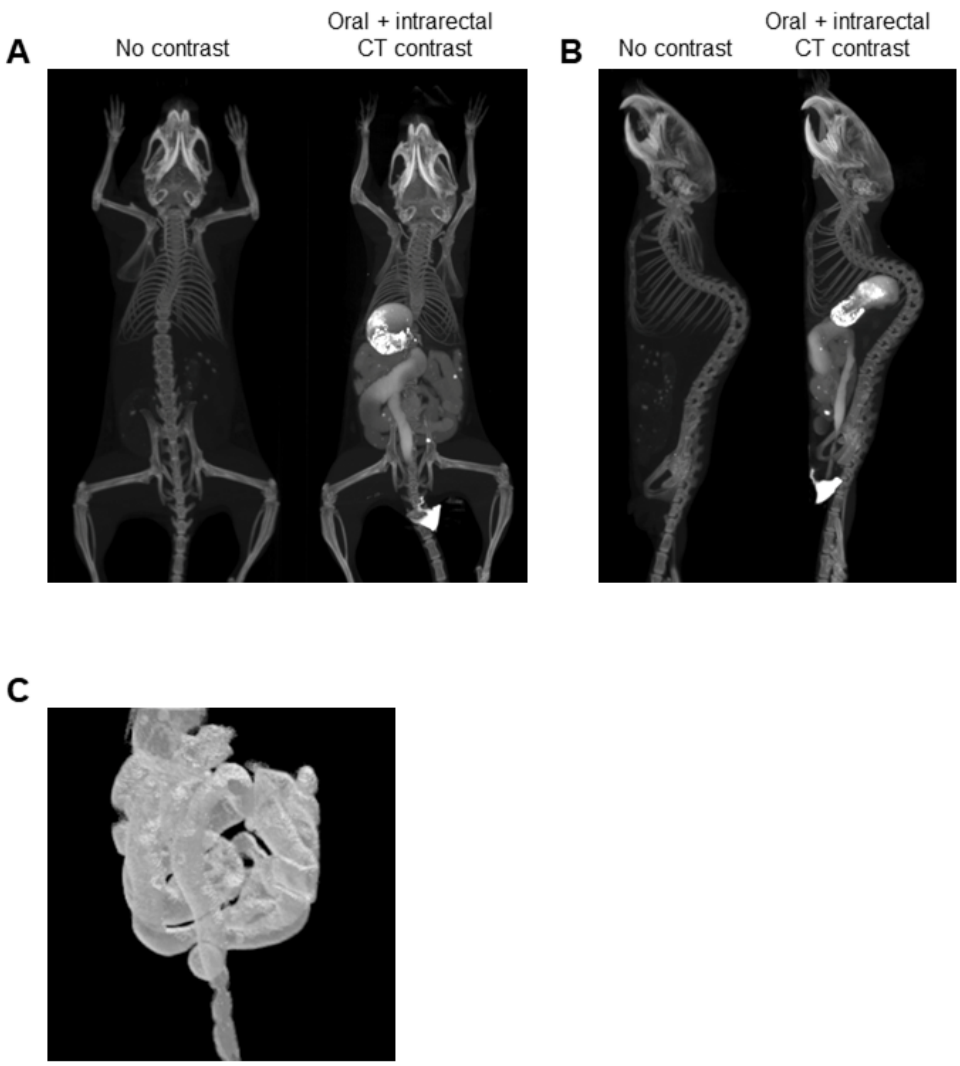

SUPPLEMENTAL FIGURE 4 CT contrast agent-assisted delineation of intestines

Oral and intrarectal CT contrast, administered prior to scanning, aided in visualizing the folds of the intestines. (A, B) Example CT images of mice treated with no contrast or with both oral and intrarectal CT contrast agent. (A) 25 mm coronal MIP, (B) 25 mm sagittal MIP. (C) Rendering of a three-dimensional isocontour ROI drawn around the entire gut based on CT intensity, including colon, cecum, small intestine, and portion of stomach. The coronal view is displayed.

SUPPLEMENTAL TABLE 1: *Ex vivo* biodistribution, % injected dose/gram

Percent injected dose per gram (%ID/g)

	Control			DSS		
	Mean	SD	n	Mean	SD	n
Blood	0.6	0.1	8	0.5	0.2	8
ILN	126.4	68.0	6	108.5	65.3	7
ALN	72.7	33.2	7	80.9	69.3	7
Spleen	123.6	18.2	8	106.1	47.4	8
Thymus	3.4	1.9	8	6.0	5.1	8
Liver	11.2	3.0	8	14.9	5.2	8
Kidney	99.6	28.8	8	114.1	36.4	8
Heart	1.6	0.5	8	2.3	1.0	8
Lung	3.2	1.9	8	2.8	0.7	8
Muscle	0.5	0.2	8	0.6	0.3	8
Femur	13.7	4.5	8	9.0	2.2	8
Tail	8.8	7.3	8	10.2	8.7	8
Carcass	1.4	0.3	8	1.5	0.2	8
Stomach	0.9	0.1	8	1.4	0.7	8
Small Int	5.9	1.5	8	5.1	1.6	8
Cecum	4.3	2.1	6	13.5	9.6	8
Colon	3.1	1.0	6	9.1	6.0	8
MLN	56.9	24.3	8	61.7	56.0	8

Activity present in blood and organs from DSS-treated mice was compared to those from control mice 26 h post-injection of ^{89}Zr-malDFO-GK1.5 cDb. Abbreviations: axillary LN (ALN), inguinal LN (ILN), mesenteric LN (MLN). No significant differences were found between the groups in any organ.